Biopharmaceutics & Drug Disposition

WILEY

ORIGINAL ARTICLE

Multifaceted Evaluation of Nano Encapsulated Polymeric Scopoletin Against HT-29 Colon Cancer Cells

Kunnathur Murugesan Sakthivel[1] | Rajan Radha Rasmi[2] | Kalavathy Murugan Kumar[3] | Kavitha Thangavelu[4] | Loganathan Chandramani Priya Dharshini[2] | Anitha Nagarajan[1] | Balasubramanian Ramesh[1]

[1]Department of Biochemistry, PSG College of Arts & Science, Coimbatore, Tamil Nadu, India | [2]Department of Biotechnology, PSG College of Arts & Science, Coimbatore, Tamil Nadu, India | [3]Department of Bioinformatics, Pondicherry University, Pondicherry, India | [4]Department of Chemistry, PSG College of Arts & Science, Coimbatore, Tamil Nadu, India

Correspondence: Balasubramanian Ramesh (rmbiochempsgcas@gmail.com)

Received: 21 December 2024 | **Revised:** 12 July 2025 | **Accepted:** 30 July 2025

Funding: Teachers Associateship for Research Excellence (TARE) by DST-ANRF (Department of Science and Technology—Anusandhan National Research Foundation), Govt of India (Ref No: TAR/2023/000019 dated 09/01/2024).

Keywords: cancer | colorectal adenocarcinoma | docking | HT-29 | nanoencapsulation | scopoletin

ABSTRACT

In the sphere of medical research, nanoencapsulated polymeric drugs in biological circumstances are an intriguing issue for therapeutical diagnosis. The nanoprecipitation approach was employed in this study to synthesis the nanoencapsulated polymeric scopoletin (NEP-Sc) and tested its effect against the HT-29 cell line (human colorectal adenocarcinoma cells). Further, the synthesized NEP-Sc was then characterized by ultra-visible spectroscopy (UV–Vis), Fourier transform infrared spectroscopy (FTIR), X-ray diffraction (XRD), field emission scanning electron microscopy (FE-SEM) with energy dispersive X-ray analysis (EDAX), and dynamic light scattering (DLS) analysis. All the analysis confirmed the effective synthesis of NEP-Sc. The synthesized NEP-Sc was validated as anticancer drug through the conventional MTT assay, neutral red uptake assay, apoptosis assay using AO/EB and lactate dehydrogenase assay and trypan blue assay against HT-29 cells. The docking studies of scopoletin with multiple genes were also carried out using the PyRx—virtual screening tool. The findings indicated that increase in concentration of NEP-Sc exhibited dose dependent action of cell death against the HT-29 colon cancer cells. To summarize, the observed results of anticancer and computational modeling studies underscores the therapeutic potential of NEP-Sc in treating colon cancer.

1 | Introduction

Colon cancer is the third chronic health condition in human population (da Paz et al. 2012). It originates at sites of bowel lining, extending towards the bowel wall and beneath the muscles (Datta et al. 2016). The pathogenesis of colon cancer may arise due to (i) genetic and epigenetic variation, (ii) abnormal proliferation of cells leading to cancer at morphological as well as molecular levels, (iii) loss of gene stability, and (iv) hereditary (Kheirelseid et al. 2013; Hutchinson et al. 2015). There are numerous targeted therapeutics against colon cancer that are currently approved and some under clinical trials which show improved efficacy and pave way for successful treatment and provides better quality of life to individuals. Although combinatorial therapies such as radiotherapy and chemotherapy are more common for completely eliminating cancer, there are numerous side effects which may be detrimental to patients (Mohammadinejad et al. 2015). Therefore, alternative therapeutics which are derived from natural compounds may prove be safe and efficient toward replacing conventional chemotherapeutic approaches with minimal side effects (Oršolić et al. 2005).

Scopoletin (Sc) (7-hydroxy-6-methoxy coumarin), a phenolic coumarin belonging to phytoalexin group is one of the potent

compounds with a molecular weight of 192 g/mol and appears to be yellow crystalline. Sc is reported to play a role in several important biological functions biological functions (Joshi et al. 2021; Sakthivel et al. 2022). Sc has proven to be beneficial compound against cancer, inflammation and hepatoprotective efficacy along with its role in gastric ulcer and colon injuries (Asgar et al. 2015; Mogana et al. 2013; Tabana et al. 2016; Kang et al. 1998; Manhattanadul et al. 2011).

Nanotechnology paved a wide range of innovative nanoparticles or materials to treat cancer (Brar et al. 2021). The efficient nanomaterial synthesis aids in the enhanced performance in diagnosis, screening and therapeutic applications in colon cancer (Gulbake et al. 2016). The incorporation of chemical compound with polymeric nanoparticles improves the mechanical performance significantly. Nano modified compounds are biocompatible, biodegradable, have high stability, high solubility, and increase the volume to surface ratio of the polymer with the drug (Gelperina et al. 2005; Thangavelu et al. 2021; Thangavelu and Zou 2022; Prisciandaro et al. 2023). Nanoformulations are more effective as they can deliver potent drugs more accurately to the targeted tissue which may reduce potential toxic side effects.

The objective of the present work is preparation of nano-encapsulated polymeric scopoletin (NEP-Sc) using nano-precipitation technique and characterized by UV spectroscopy, Fourier transform infrared spectroscopy, X-ray diffraction, scanning electron microscopy, particle size analysis, poly-dispersity index, and zeta potential analysis. Further the efficacy of the prepared and characterized NEP-Sc was evaluated for antitumor activity in vitro. In silico molecular docking analysis were performed to unveil the mechanism of interaction of Sc with the cancer and oxidative stress markers.

2 | Materials and Methods

2.1 | Materials

Scopoletin (> 99% purity, molecular weight 192.17), Poly (D,L-lactide-*co*-glycolide) (PLGA), Poly (vinyl alcohol) (PVA) were purchased from Sigma-Aldrich (USA). DMSO, fetal bovine serum (FBS), phosphate-buffered saline tablets (pH 7.4), 0.25% trypsin-EDTA, and DMEM medium were purchased from Fisher Scientific (USA). All solvents and chemicals used for the study were of analytical grade.

2.2 | Preparation of Nanoencapsulated Polymeric (PLGA-PVA) Scopoletin (NEP-Sc)

NEP-Sc was prepared by nano precipitation technique with slight modifications (Sulaiman et al. 2018) (Figure 1). Typically, 5 mg of pure Sc and 10 mg of poly lactic-co-glycolic acid (PLGA) in 2.5 mL of dimethyl sulfoxide (DMSO) was added to make Sc/PLGA in an organic approach. 10 mg of poly vinyl alcohol (PVA) was added into 5 mL of distilled water at 75°C to obtain the aqueous phase. The Sc/PLGA mixture was injected in a dropwise manner (0.5 mL/min) into 10 mL of PVA stabilizer solution at 25°C under magnetic stirring. Subsequently, the mixture was agitated thoroughly in a sonic bath for few mins. After complete evaporation, it was centrifuged at 15,000*g* for 15 min to remove free molecule from unbound stabilizer. The supernatant was collected and freeze-dried using lyophilizer (Chen and Wang 2019).

2.3 | Characterization of Sc-Encapsulated PLGA-PVA Nanoparticles

2.3.1 | UV Spectroscopy Analysis

UV-visible spectra of Sc, PLGA-PVA and NEP-Sc were recorded with Shimadzu UV-1700 Pharma spectrophotometer in the wavelength range of 200–800 nm. Before measurement, the samples were diluted with aqueous solution and calibration curve was generated.

2.3.2 | Fourier Transform Infrared Spectroscopy Analysis (FTIR)

The functional group present in the prepared nanoparticles was analyzed by FTIR spectrometer (IR Affinity-1, Shimadzu, Japan) over a range of 4000 to 650 cm^{-1}. FTIR spectrum were recorded using Nicolet Nexus operated at a resolution of 16 cm^{-1}.

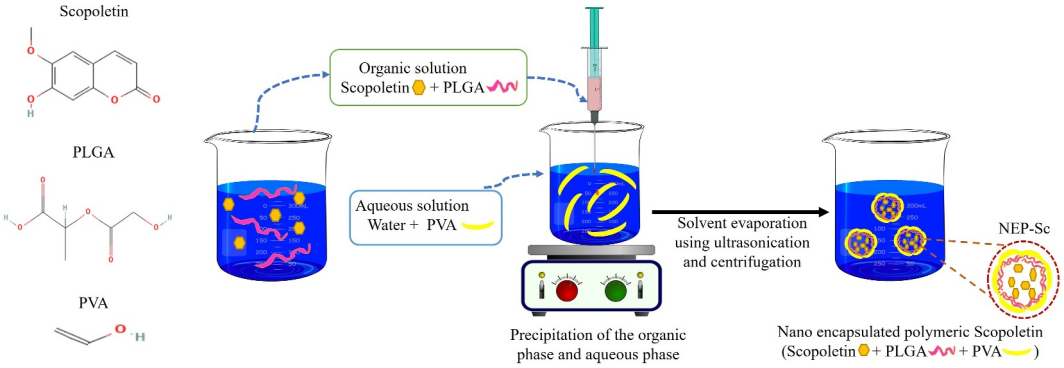

FIGURE 1 | Schematic illustration of the preparation of NEP-Sc. The Sc/PLGA solution was dropwise injected into a PVA stabilizer solution under magnetic stirring, followed by sonication for stabilization. After centrifugation and removal of unbound molecules, the nanoparticles were collected and freeze-dried.

2.3.3 | X-Ray Diffraction (XRD) Analysis

XRD patterns of Sc, PLGA-PVA and NEP-Sc were obtained using a very high-resolution Cu-K_α radiation diffraction system (Empyrean, Malvern Panalytical multipurpose diffractometer). The samples were exposed to Cu Kα radiation of wavelength 1.54 Å operating at a voltage of 45 kV and current of 30 mA. NEP-Sc was analyzed in the 2θ angle range of 4°–89°.

2.3.4 | Field Emission Scanning Electron Microscopy (FESEM) Analysis

The size, shape, morphology and uniformity of nanoparticles were performed with the use of FESEM, using a Carl Zeiss (USA) system (Model: Sigma with Gemini column) operated at a 10.0 kV accelerating voltage.

2.3.5 | Energy Dispersive X-Ray (EDAX) Analysis

Elements present in the pure Sc, PLGA-PVA and NEP-Sc was conducted using energy dispersive X-ray (EDAX) detector using a Nano Xfalsh detector model of the Bruker (German) system. Elemental analysis was focused on point scan, area scan, line scan and elemental mapping operated at 20.0 kV.

2.3.6 | Particle Size, Polydispersity Index (PDI) and Zeta Potential (ZP) Analysis

The size distribution, PDI and ZP of the polymeric micelles was obtained using laser doppler anemometry (LDA), Zetasizer, and Nano-ZS90 instrument (Malvern Instruments Ltd., Malvern, UK) at a temperature of 25°C. The freeze-dried nanoparticles were diluted in ultrapure water and the data were analyzed in triplicates using automatic mode.

2.3.7 | Encapsulation Efficiency

Nanoparticles collected and precisely weighed. The yield was then computed as percentage (%) using the below given formula:

$$\% \text{ Yield} = (\text{Mass of nanoparticle obtained} / \text{Total weight of drug and polymer}) \times 100$$

The amount of scopoletin entrapped in the nanoparticles was evaluated by centrifuging scopoletin-loaded nanoparticles from a free scopoletin suspension. The acquired sample was centrifuged for 10 min at 12,500 × g, and the free scopoletin in the supernatant was measured by UV spec at 344 nm. The following equations were used to calculate the percentage EE and DL of NEP-Sc:

$$\text{Entrapment efficiency (EE\%)} = (\text{Wt of scopoletin in NPs} / \text{Wt of initial drug}) \times 100$$

$$\text{Drug loading (DL\%)} = (\text{Wt of scopoletin in NPs} / \text{Wt of NPs}) \times 100$$

2.4 | In Vitro Anticancer Activity

2.4.1 | Cell Culture

HT-29 human colorectal adenocarcinoma cells were purchased from NCCS, Pune. The cells were cultured in DMEM with 10% heat-inactivated fetal bovine serum and penicillin/streptomycin (100 U/mL penicillin and 100 μg/mL streptomycin) in a humidified incubator with 5% CO_2 at 37°C.

2.4.2 | MTT Assay

The cytotoxic activity of the prepared NEP-Sc was studied in HT-29 cells using MTT assay. Cells (HT-29 cell line) were seeded at intensity of 1×10^5 cells/mL in 96 well plates for 24 h at 37°C in CO_2 incubator. The media was changed in each well and cells were treated again with different concentrations of desired compound (5, 25, 50, 75, and 100 μg) for 24 h at 37°C in CO_2 incubator. Phosphate buffered saline (PBS) was used as negative control. After incubation, media was discarded with subsequent addition of 100 μL MTT reagent (5 mg/mL) and incubated at 37°C for 2 h. Added 100 μL of DMSO per well for 30 min at 37°C in CO_2 incubator which solubilizes the formazan crystals. This was then measured using microplate reader (Bio-rad Laboratories, USA) at 570 nm (Bahuguna et al. 2017). Cell survival was measured using the following formula:

$$\text{Survival (\%)} = \frac{\text{Mean eperimental (Optical density) value}}{\text{Mean control (Optical density) value}} \times 100$$

2.4.3 | Neutral Red Uptake (NRU) Assay

HT-29 Cells were grown for 18 h to attain a half-confluent monolayer. The spent media was discarded and treated with NEP-Sc, followed by overnight incubation. 100 μL of neutral red dye was added to each well and incubated for 2 h. The medium was removed and the cells were rinsed with 150 μL of PBS. After washing, 150 μL of neutral red was added to detain reagent and kept in a microtitre plate shaker for 10 min in order to remove the dye from cells. The absorbance of the extracted dye at 540 nm was measured in a microplate reader using blanks which contains no cells as reference (Repetto et al. 2008). The percentage of cell viability is calculated using the following equation:

$$\% \text{ Viability} = \frac{\text{Mean(Optical density) value of sample}}{\text{Mean (Optical density) value of blank}} \times 100$$

2.4.4 | Apoptosis Assay Using AO/Et-BR Fluorescent Dye

HT-29 cells were seeded at a concentration of (0.5–2.0 × 10^6 cells/mL) for 24 h at 37°C in CO_2 incubator. After

attaining approximately 70%–80%, cells were treated with the different concentration of the sample (25, 50, 75, and 100 μg) for next 24 h at 37°C in CO_2 incubator. Then, it was rinsed twice or thrice with 1 mL of PBS. 1 μL of Acridine orange (AO) (5 mg/mL) and 1 μL of ethidium bromide (EtBr) (3 mg/mL) solution was added and left for 1–2 min. Again, it was rinsed with PBS and subsequently resuspended with 50 μL of PBS. Before imaging, the stained cell suspensions are mixed gently. Placed 10 μL of sample onto a microscopic slide and examined under fluorescence microscope using a fluorescein filter and a 60× objective lens (Yashaswee and Trigun 2020).

2.4.5 | Lactate Dehydrogenase (LDH) Assay

HT-29 Cells were seeded at 1–5 × 10^4 cells/mL and incubated for 24 h at 37°C in CO_2 incubator. Each experiment groups are prepared in triplicates. Approximately 15 μL of lysis buffer was added and returned to 5% CO_2 incubator at 37°C for 45 min. Followed by centrifugation of the plate at 250*g* for 4 min, 50 μL of supernatant was transferred with addition of 50 μL of LDH assay buffer and mixed gently for 30 s. The assay was protected by covering it with a foil and incubated at 37°C for 15–30 min. After incubation, 100 μL of stop solution was added and mixed slowly. Optical density was measured between 490 and 690 nm (Chan et al. 2013). The percentage cytotoxicity was calculated using the below formula:

$$\%\ \text{Cytotoxicity} = \frac{(\text{Corrected reading from Test well} - \text{Corrected reading from untreated well})}{(\text{Corrected maximun LDH release control} - \text{corrected reading from untreated well})} \times 100$$

2.4.6 | Trypan Blue Assay (Live/Dead Cell Detection)

1 mL of sample for viability testing was centrifuged at 100 × g for 5 min. Resuspended the pellet in 1 mL of PBS. 1:1 of 0.4% trypan blue and cell suspension were mixed followed by incubation at room temperature for ~3 min. The cells were gently mixed and a drop of sample mixture was applied to the hemacytometer. The unstained (viable) and stained (nonviable) cells were counted separately and viable cell percentage was calculated using the below formula (Strober 1997).

$$\text{Viable cells (\%)} = \frac{\text{total number of viable cells per ml of aliquot} \times 100}{\text{total number of cells per mL of aliquot}}$$

2.5 | In-Silico Molecular Docking Analysis

Docking studies were carried out using PyRx—virtual screening software. The three-dimensional structure (3D) of ligands—Sc (PubChem ID: 5280460), 5-Fluorouracil (PubChem ID: 3385) and Sulfasalazine (PubChem ID: 5339) were obtained in SDF file format from PubChem database. The three-dimensional structure of the markers and proteins were obtained from the RCSB Protein Data Bank in a RDB file. Markers and proteins retrieved are as follows: cancer markers: (1) nuclear erythroid-2-related factor 2—NRF2 (PDB ID: 2LZ1), (2) Kelch-like ECH associated protein 1—Keap 1 (PDB ID: 1U6D), (3) heme oxygenase1—HO1 (PDB ID: 1N3U), (4) toll-like receptor 2—TLR2 (PDB ID: 1FYW); apoptotic markers: (1) caspase-3 (PDB ID: 3DEI), (2) BCL-XL (PDB ID: 1R2D), (3) B-cell lymphoma 2—Bcl2 (PDB ID: 5JSN), (4) BCL2 antagonist/killer 1—BAK1 (PDB ID: 2JCN); autophagy markers: (1) lysosome-associated membrane glycoprotein 3—LAMP3 (PDB ID: 4AKM), (2) microtubule-associated protein 1A/1B-light chain 3—LC3 (PDB ID: 1UGM), (3) sirtuin (Silent mating type information regulation 2 homolog)—SIRT1 (PDB ID: 4IG9); inflammatory proteins: (1) signal transducer and activator of transcription 1—STAT1 (PDB ID: 2WWT), (2) tumor necrosis factor-α—TNF-α (PDB ID: 1A8M), (3) cytochrome C oxidase subunit 2—COX2 (PDB ID: 3VRJ), (4) inducible nitric oxide synthase—iNOS (PDB ID: 1NSI). All these receptors and ligands were used to conduct a thorough investigation into the interaction and binding mechanism of the receptor-ligand complex. Using PyRx-Autodock vina, the ligands and receptor PDB file formats were converted to the AutoDock Pdbqt format. Using the Molegro Molecular Viewer Executable program, the receptors were pre-docked, followed by the removal of water molecules and addition of hydrogen atoms. PyRx-Autodock vina software was used for molecular docking studies. The docking results of the best pose of the ligand–receptor complexes based on hydrogen bonds and electrostatic and hydrophobic interactions were expressed as binding energy values (kcal/mol). PyMOL software was used to visualize H-bond interactions, binding affinities, binding atoms on the ligands and receptors and three-dimensional representations of ligand–receptor complexes, whereas Discovery studio visualizer was used to visualize two-dimensional graphical illustrations and interacting amino acids of ligand–binding interactions (Gul et al. 2019).

2.6 | Statistical Analysis

Statistical analysis was done using one-way ANOVA with GraphPad Prism 3 software. Values were represented as mean ± SD of triplicates.

3 | Results

3.1 | Characterization of NEP-Sc

The synthesis of NEP-Sc was prepared by nano precipitation technique was shown in Figure 1. Further, NEP-Sc was characterized using the following techniques: UV-visible spectroscopy, FTIR analysis, XRD analysis, FESEM analysis, EDAX analysis, particle size, PDI, and ZP analysis.

3.1.1 | UV-Visible Spectroscopy Analysis

The light transmittance of the NEP-Sc was studied by recording the UV-Visible spectra from 200 to 800 nm, which are shown in Figure 2. The pure Sc showed the peak in the range of 344.50 and 294.00 nm, PLGA-PVA polymeric nanoparticles showed peak at 287.50 nm and NEP-Sc showed a combined peak at the range of 342 and 294 nm.

3.1.2 | FTIR Analysis

The FTIR spectrum of Sc, PLGA-PVA nanoparticles and NEP-Sc is shown in Figure 3A–C. Figure 3A shows clear peaks of Sc in the –O–H, C=O and C–O stretching regions at 3379, 1635, and 1234 cm^{-1} respectively. Peaks at 1496 and 1373 cm^{-1} attributed to aromatic C=C stretching. Several peaks between 2900 and 2330 cm^{-1} reconciled with C–H stretching of methyl groups. Terminal C=C alkyne, isothiocyanate (-NCS), C=C alkyne stretch were responsible for the formation of the peaks at 2106, 2052, and 1635 cm^{-1}, respectively. Figure 3B shows the FTIR analysis of PLGA-PVA nanoparticles. The peaks at 3356 cm^{-1} attributed to OH stretching vibrations at the end group. Peaks at 3294, 2360, and 2044 cm^{-1} contributed to stretching vibrations of C–H. C=O stretch, bending vibrations of CH_2 and CH_3 groups were corresponds at peaks 1635, 1365, and 1219 cm^{-1} respectively. Peaks between 1010 and 941 cm^{-1} corresponds for the C–H bends. Figure 3C shows the FTIR peaks of NEP-Sc. Peaks obtained for both Sc and PLGA-PVA nanoparticles were combined to form Sc-encapsulated PLGA-PVA nanoparticles.

3.1.3 | XRD Analysis

XRD was evaluated for the identification of crystalline nature of scopoletin, PLGA + PVA and nano-encapsulated scopoletin. XRD examination of drug, polymer and drug loaded polymeric nanoparticles was examined (Figure 4). The existence of sharp and intense peaks in the diffractogram of pure scopoletin demonstrates its crystalline structure, but no sharp peaks were obtained in the case of PLGA-PVA, showing its amorphous nature. The drug and drug-loaded NPs were less crystalline form and exhibited less intense peaks at PLGA-PVA exhibiting the characteristic intense peak at 2θ approximately at 12.52°, 20.82°, and 42.32° and pure scopoletin exhibiting the characteristic intense peaks at 2θ approximately at 13.50°, 28.75°, 41.53°, and 48.65°. The physical mixture exhibited partially sharp crystalline peaks with high broad peaks present in nanoencapsulated polymeric scopoletin, indicated that the NPs were amorphous and lacked crystalline peaks.

3.1.4 | FESEM Analysis

FESEM evaluates the size, morphology and uniformity of Sc, PLGA-PVA polymers and NEP-Sc as shown in Figure 5. Pure Sc

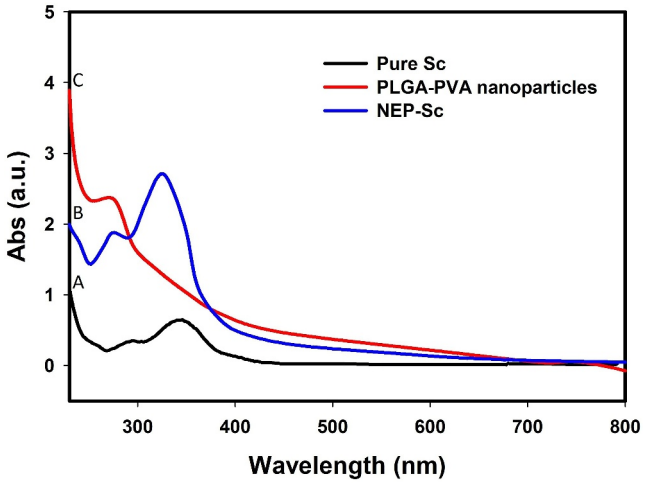

FIGURE 2 | UV spectroscopy analysis. (A) Pure Sc. (B) PLGA-PVA nanoparticles. (C) NEP-Sc. Pure Sc exhibited peaks at 344.50 and 294.00 nm, while PLGA-PVA nanoparticles showed a peak at 287.50 nm. The NEP-Sc spectrum displayed combined peaks at 342.00 and 294.00 nm, indicating successful nanoparticle formation.

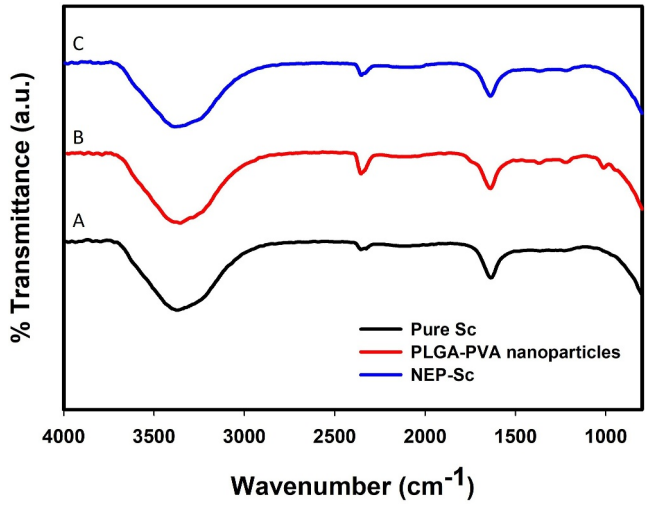

FIGURE 3 | FTIR spectroscopy analysis. (A) Pure Sc. (B) PLGA-PVA nanoparticles. (C) NEP-Sc. (A) The FTIR spectrum of Sc showed characteristic peaks for –O–H, C=O, and C–O stretching at 3379, 1635, and 1234 cm^{-1}, respectively, along with aromatic C=C stretching at 1496 and 1373 cm^{-1}. (B) PLGA-PVA nanoparticles exhibited OH stretching at 3356 cm^{-1} and C=O, CH_2, and CH_3 group vibrations at 1635, 1365, and 1219 cm^{-1}, respectively. (C) NEP-Sc combined characteristic peaks of Sc and PLGA-PVA nanoparticles, confirming successful encapsulation.

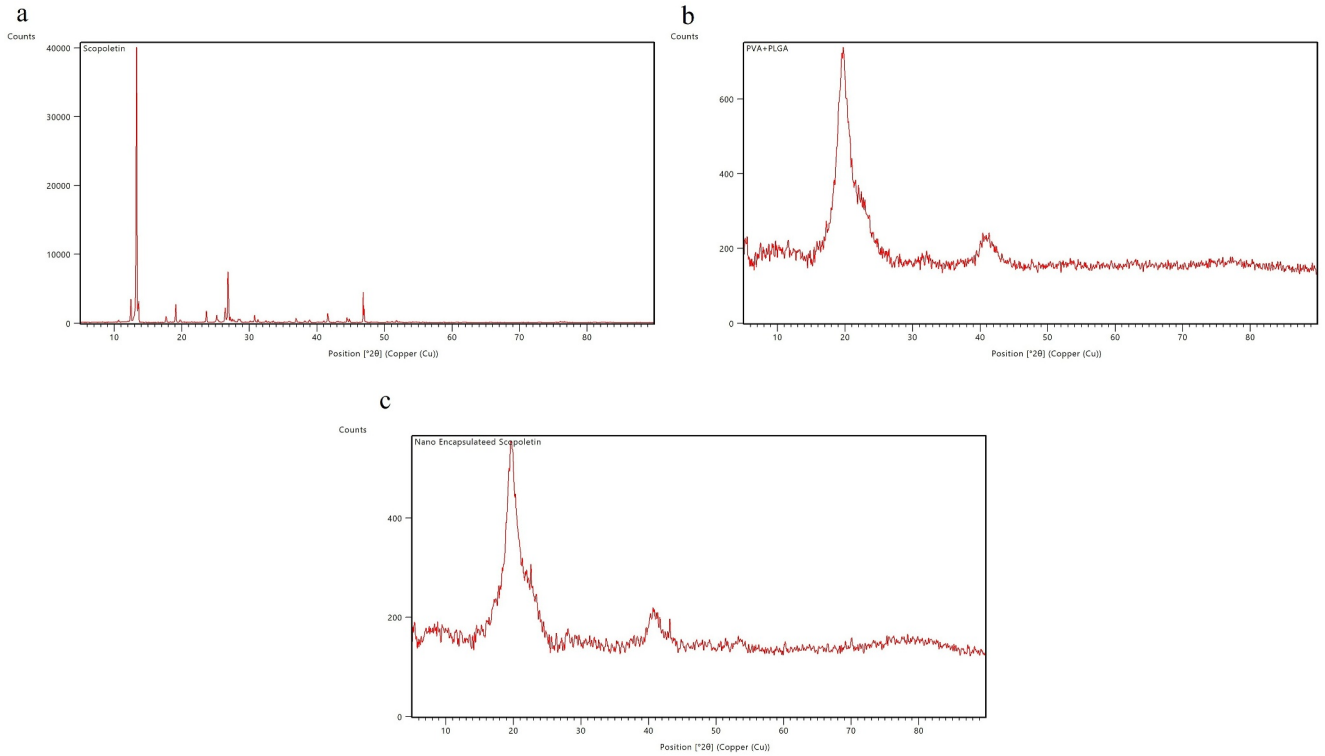

FIGURE 4 | XRD analysis. (a) Pure Sc. (b) PLGA-PVA nanoparticles. (c) NEP-Sc. The diffractogram of pure Scopoletin displayed sharp and intense peaks, confirming its crystalline nature, while PLGA-PVA showed an amorphous profile with no sharp peaks. NEP-Sc exhibited reduced crystallinity with broad peaks, combining characteristics of both Scopoletin and PLGA-PVA, indicating successful nanoencapsulation.

was observed with irregular arrangement of particles, rectangular, and shows crystalline nature; PLGA-PVA polymeric nanoparticles shows smooth morphology with size ranging between 44.04 and 49.89 nm, whereas the combined and modified form of NEP-Sc witnessed that major particles showed defined structural arrangement, spherical, and with smooth surfaces, with diameters ranging between 29.30 and 38.09 nm. The change in size of NEP-Sc is due to electrostatic repulsion force and steric hindrance between the polymer chains on the NEP-Sc. NEP-Sc obtains spherical shape and expected to enhance the release of scopoletin from the matrix polymer and transport of Scopoletin in the body.

3.1.5 | EDAX Analysis

The chemical composition and the concentration within the materials were determined using EDAX analysis. Figure 6a–c shows a homogenous dispersion of elemental composition in Pure Sc, PLGA-PVA and NEP-Sc. The initial chemical composition of scopoletin was evaluated, and it matched the final NEP-Sc in combination with PLGA-PVA. The absence of contaminants in the result also indicated the purity of the sample. The chemical analysis of NEP-Sc validated the possibility of synthesis via nanoprecipitation technique.

3.1.6 | Particle Size, PDI and ZP

The mean diameter, PDI, and ZP of the NEP-Sc were measured using laser doppler anemometry (LDA), Zetasizer, and Nano-ZS90 instrument (Malvern Instruments Ltd., Malvern, UK) at a temperature of 25°C. PDI value is a ratio that provides information about the homogeneity and width of particle size distribution. It was below 0.382 for NEP-Sc, which indicates the narrow size range distribution around 199.9 nm. The size range of pure Sc and PLGA-PVA nanoparticle are 161.1 and 171.4 nm, respectively. ZP of the particles has a considerable play in assessing the strength and stability of a colloidal dispersion. It reflects the surface properties of nano-sized nanoparticles, was −27, −14.9, and −15.5 mV for Sc, PLGA-PVA nanoparticle and NEP-Sc, respectively. It fell within the range of −10 to −30 mV for well-stabilized nanoparticles (Table 1) (Figures 7 and 8).

3.1.7 | Percentage Yield, Entrapment Efficiency and Drug Loading

The yield coefficient, entrapment efficiency and drug loading capacity were found to be $52 \pm 0.8\%$, $89.6 \pm 0.9\%$, and $68.9 \pm 1.2\%$, respectively. NEP-Sc has good encapsulation efficiency, with no

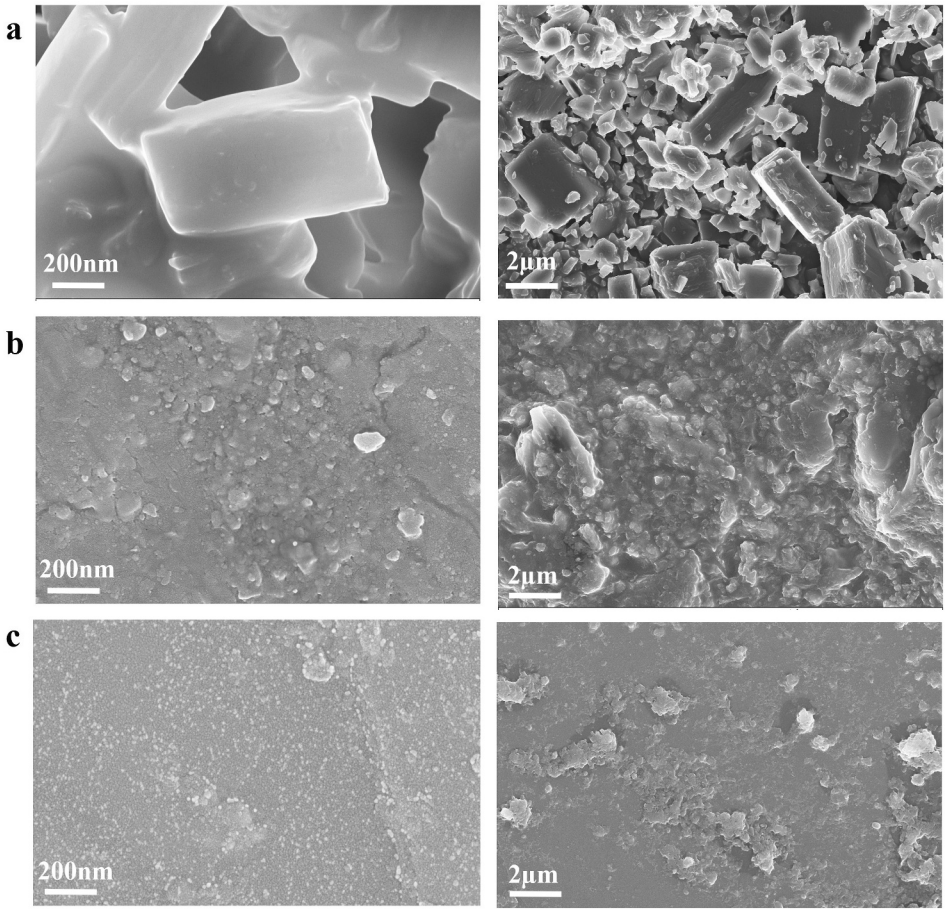

FIGURE 5 | SEM analysis. (a) Pure Sc. (b) PLGA-PVA nanoparticles. (c) NEP-Sc. Sc displayed irregular, rectangular particles with a crystalline nature. PLGA-PVA nanoparticles exhibited smooth morphology with sizes ranging from 44.04 to 49.89 nm. NEP-Sc showed well-defined, spherical particles with smooth surfaces, and sizes between 29.30 and 38.09 nm, attributed to electrostatic repulsion and steric hindrance, enhancing Scopoletin release and transport.

change in encapsulation efficiency due to polymer saturation after a given period of time.

3.2 | In Vitro Anticancer Activity

3.2.1 | MTT Assay

The MTT assay [3-(4, 5-dimethylthiazol-2-yl)-2, 5-diphenylte trazolium bromide], which utilizes the metabolic activity of cells to assess the viability, was employed to evaluate the cytotoxic effect of NEP-Sc on HT-29 cells. After 24 h of contact, the NEP-Sc showed significant cytotoxicity to HT-29 cells with a cytotoxicity percentage of 61% and cell viability percentage of 38.2%. Moreover, cell viability exhibited a dose-dependent response, meaning higher NEP-Sc concentrations resulted in greater cytotoxicity. In addition, we calculated the IC_{50} value of 59.17 µg/mL, suggest that NEP-Sc holds promise as a potential therapeutic strategy for colon cancer (Figure 9a).

3.2.2 | Neutral Red Assay

The neutral red assay of HT-29 cell line was used to examine the cell viability following exposure to NEP-Sc. The results demonstrated a concentration-dependent effect of NEP-Sc on HT-29 cell viability. At a low concentration (25 µg), cell viability was found to be 84.67% which decreased to 38% at a higher concentration (100 µg). This observed decrease in viability suggests that NEP-Sc induced cytotoxicity in HT-29 cells (Figure 9b).

3.2.3 | Apoptosis/Necrosis by LDH Assay

Apoptosis/Necrosis was observed using nonradioactive LDH assay which depends upon the deduction of tetrazolium salt MTT in a NADH-coupled enzymatic reaction. LDH enzyme release in the media is an indication of cell membrane damage leading to apoptosis of cancer cells. HT-29 cells treated with increasing concentrations (25–100 µg) of NEP-Sc showed an

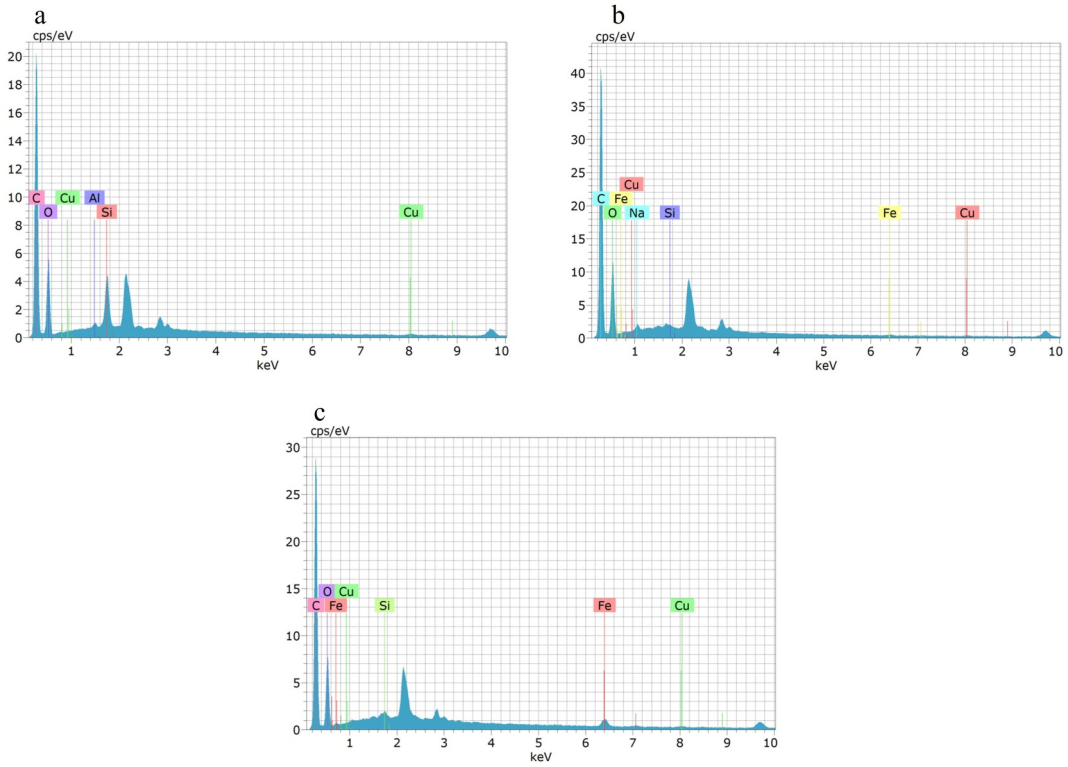

FIGURE 6 | EDAX analysis. (a) Pure Sc. (b) PLGA-PVA nanoparticles. (c) NEP-Sc. The elemental composition showed homogeneous dispersion in all samples, with NEP-Sc retaining the chemical composition of Scopoletin in combination with PLGA-PVA. The absence of contaminants confirmed the purity of the samples, validating the nanoprecipitation synthesis technique.

TABLE 1 | Particle size (PS), polydispersity index (PDI), zeta potential (ZP) analysis of Sc, PLGA-PVA nanoparticles and NEP-Sc.

Sample	Size (nm)	PDI	ZP (mV)
Sc	161.1	0.382	−27
PLGA-PVA nanoparticles	171.4	0.891	−14.9
NEP-Sc	199.9	0.782	−15.5

increased release of LDH at higher concentrations with 78.1% of cytotoxicity compared to untreated cells (Figure 9c).

3.2.4 | Trypan Blue Assay (Live/Dead Cell Detection)

Trypan blue assay was examined to check for live/dead cell detection in HT-29 cell line. At low concentration (25 μg), the cell viability was found to be 89.78% which decreased to 35.20% at higher concentration (100 μg). Viability of HT-29 cells decreased with increased concentrations of NEP-Sc (Figure 9d).

3.2.5 | Apoptosis Assay by AO/EB Fluorescent Dye

To assess the potential of NEP-Sc to induce apoptosis, an acridine orange/ethidium bromide (AO/EB) staining assay was performed on HT-29 cells. We observed a concentration-dependent increase in apoptosis with NEP-Sc treatment, which significantly correlated with a decrease in cell viability (Figure 9e).

3.3 | In-Silico Molecular Docking Analysis

A total of 15 marker genes were taken for the study. Out of which 4 genes belongs to cancer markers, 4 apoptotic markers, 3 autophagic markers and 4 inflammatory markers. Molecular docking studies were taken froth using PyRx software to determine the interactivity amid the standard and test drug against colon associated cancer and inflammation respectively. Among the four cancer markers, Sc shows the highest binding affinity for Keap-1 gene with −7.0 kcal/mol. In four of the apoptotic markers, Caspase-3 with Sc has the higher binding score of −6.3 kcal/mol. LC-3, an autophagy marker among 3 other marker genes shows higher binding energy with Sc of −6.1 kcal/mol. Among the four inflammatory genes, Sc shows higher binding affinity with COX2 of −6.9 kcal/mol. The greater the negative value during docking indicated the higher binding force amidst the compound and marker gene. Figures 10 and 11 depicts the docking image. The score for all higher interacting genes with key proteins were ≥ −5.0 kJ/mol, implying that this compound employs a vigorous binding effect (Tables 2 and 3). Binding energy calculation and Percentage of resemblance of all genes compared to standard and listed in the Table 4.

4 | Discussion

Nano modification system is a technique where the chemical drug compound is surrounded by polymer materials which has numerous advantages including enhanced mechanical properties, high stability, increased solubility, and magnified physiochemical properties (Khuda-Bukhsh et al. 2010). For proper

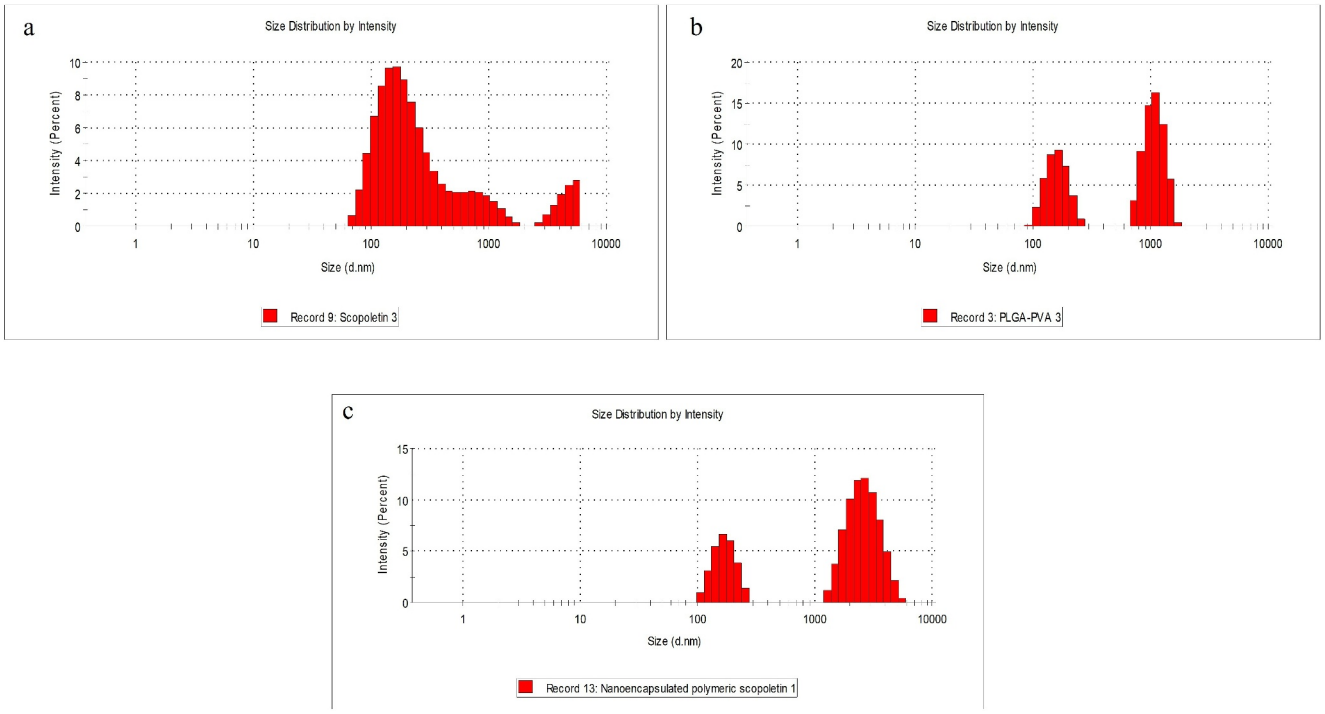

FIGURE 7 | Particle size distribution analysis. (a) Pure Sc. (b) PLGA-PVA nanoparticles. (c) NEP-Sc. The particle size of NEP-Sc was measured as 199.9 nm, Pure Sc (161.1 nm) and PLGA-PVA nanoparticles (171.4 nm). A PDI value of 0.382 for NEP-Sc indicates a narrow size range and good homogeneity.

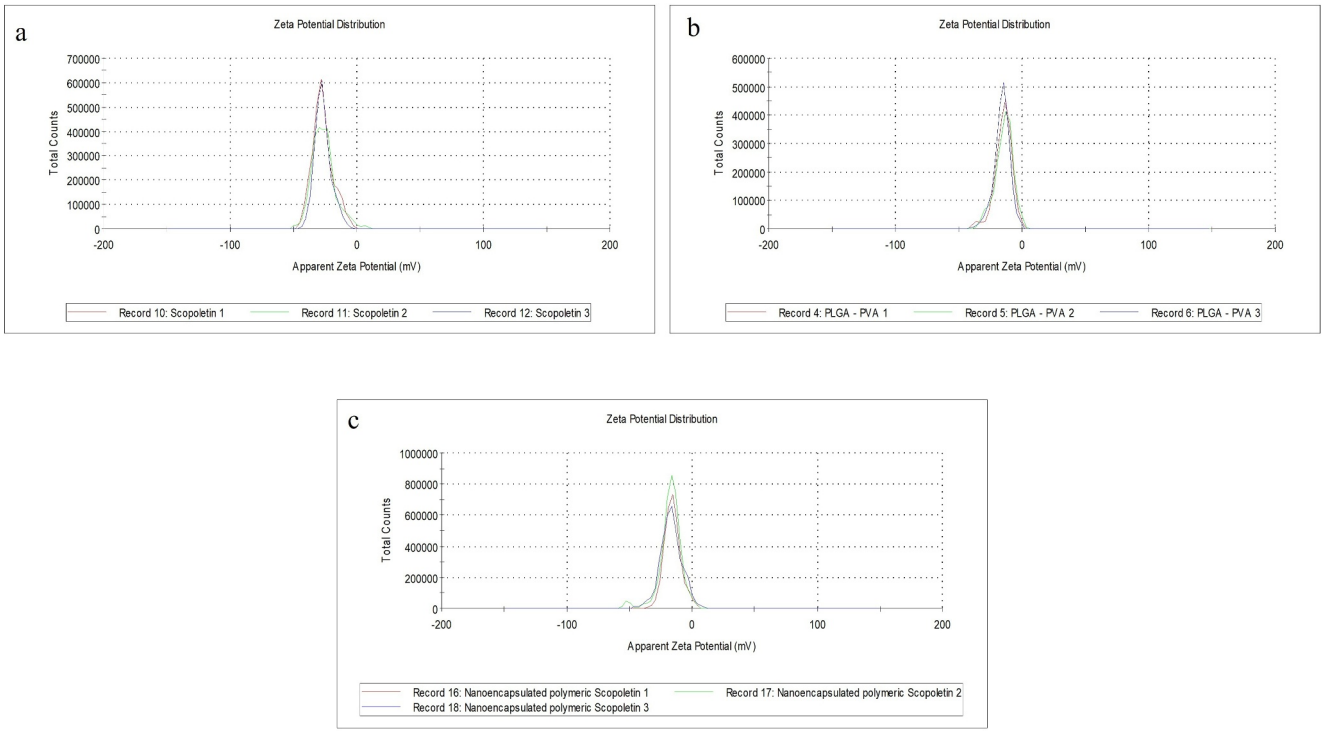

FIGURE 8 | Zeta potential analysis. (a) Pure Sc. (b) PLGA-PVA nanoparticles. (c) NEP-Sc. The ZP values were −27 mV for Sc, −14.9 mV for PLGA-PVA and −15.5 mV for NEP-Sc. These values fall within the range of −10 to −30 mV, indicating well-stabilized nanoparticles.

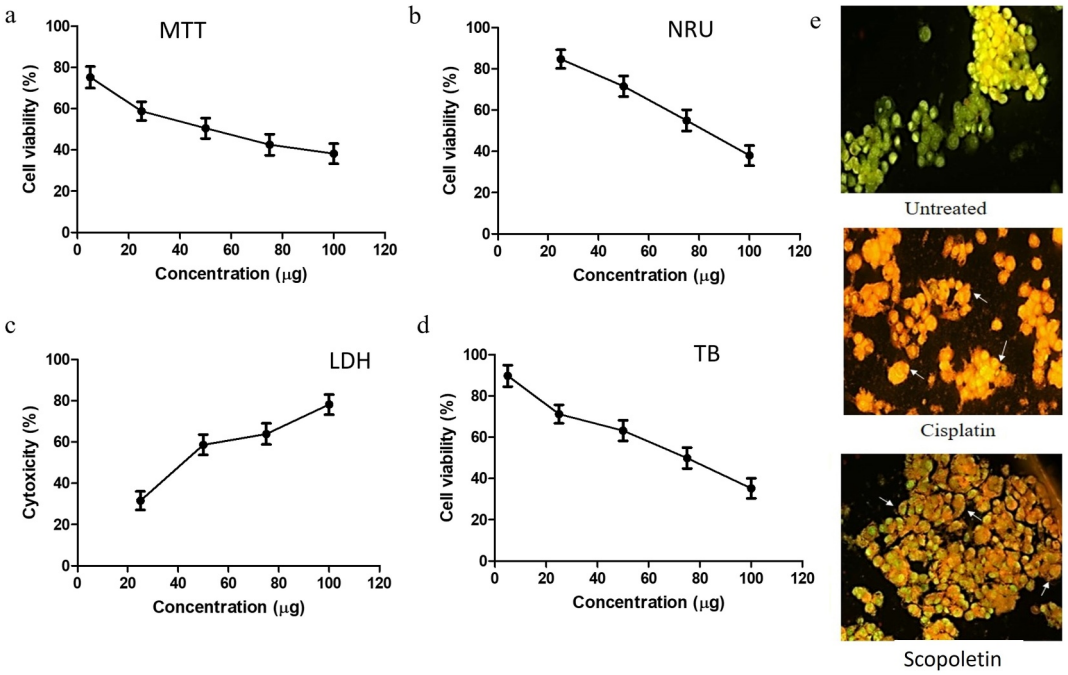

FIGURE 9 | Effect of NEP-Sc on HT-29 cells. (a) Graphical representation of MTT assay. NEP-Sc reduced the viability of HT-29 colon cancer cells. Cell viability was measured using the MTT assay. (b) Graphical representation of neutral red uptake (NRU) assay. NEP-Sc concentration-dependently reduces the viability of HT-29 colon cancer cells represented using neutral red uptake assay. (c) Lactate dehydrogenase assay. (d) Trypan blue assay. Values are represented as mean ± SD. (e) Apoptosis detection using Acridine Orange/Ethidium Bromide: Control; the loss of nuclear shape and the expansion of nuclear material; apoptotic bodies containing the fragmented DNA (early apoptosis) were visible, appearing as green fluorescent patches and hypersegmented nuclei were observed.

release of the compound, polymeric nanoparticles obtained from biodegradable and biocompatible polymers are used (Allémann et al. 1993; Sallal et al. 2020). PLGA and PVA are used as polymers due to its biodegradability, biocompatibility and less toxicity (Sulaiman et al. 2018). In the present article, NEP-Sc is prepared, characterization and evaluated for anti-tumor assays. Molecular docking of Sc was performed against 15 tumor related proteins.

NEP-Sc was prepared using nano precipitation technique as described by Sulaiman et al. (2018). The Sc was loaded within PLGA-PVA nanoparticles with 99.49% entrapment efficiency. UV characterization of NEP-Sc showed a combined peak at the range of 342.00 and 294.00 nm which is similar to pure Sc and PLGA-PVA nanoparticles, respectively. FTIR analysis of NEP-Sc shows the combination of peaks obtained for pure Sc and PLGA-PVA nanoparticles. FESEM analysis of modified NEP-Sc revealed that most of the particles exhibited well-arranged structural morphology displaying smooth and sphered surfaces ranging amid 29.30–38.09 nm. Elemental analysis revealed that the initial element analysis in Sc and PLGA-PVA were matched with the result of NEP-Sc (Wei et al. 2017). The physicochemical properties of Sc are more important in therapeutics that depends on numerous aspects including size, ZP, and PDI of the compound. PDI value is essential as it suggests homogenous distribution in NEP-Sc (de Araujo Lopes et al. 2013). ZP values are generally more than +30 and < −30 mV which are stable as there is low particle aggregation. In our study, zeta potential value of NEP-Sc lies in the range of −10.7 mV which is considered to be a stable nano modified compound in similar to study conducted by de Araujo Lopes et al. (2013). Both particle size and polydispersity index of nano modified Sc lies in the range between pure Sc and PLGA-PVA nanoparticles. The characterized NEP-Sc was further evaluated for anti-tumor assays.

MTT assay and NRU assay was carried out to examine the viability of HT-29 cells. Both the cell viability assays show decrease in cell survival with increase in concentration of the *Zanthoxylum armatum* extracts against MCF-7, MDA-MB-468, and Caco-2 cancer cell line. Similar results were observed in our study which shows decline in survival of cells with increase in concentration of the compound (Alam et al. 2017). Apoptosis was detected using AO/EtBr staining and LDH assay. AO/EtBr staining assay was performed which shows gradual loss of nuclear shape followed by DNA fragmentation simultaneously leading to hyper segmented nuclei with increase in concentration of nano encapsulated Sc. Our observed result showed nuclear shape loss with apoptotic bodies formation along with DNA fragmentation and hyper segmented nuclei as shown in similar study by Yu et al. (2015). Release of LDH in media, is an indication showing the loss in membrane integrity which causes apoptosis/necrosis. Therefore, LDH assay was carried out to evaluate the cytotoxicity of NEP-Sc. Recent study by Reheman et al. (2020), observed the escalation in discharge of LDH in media of HeLa cells with dosage rise of the compound [Cu (PMPP-SAL)(EtOH)]. Our study also been observed with increase in concentration of NEP-Sc increases LDH release

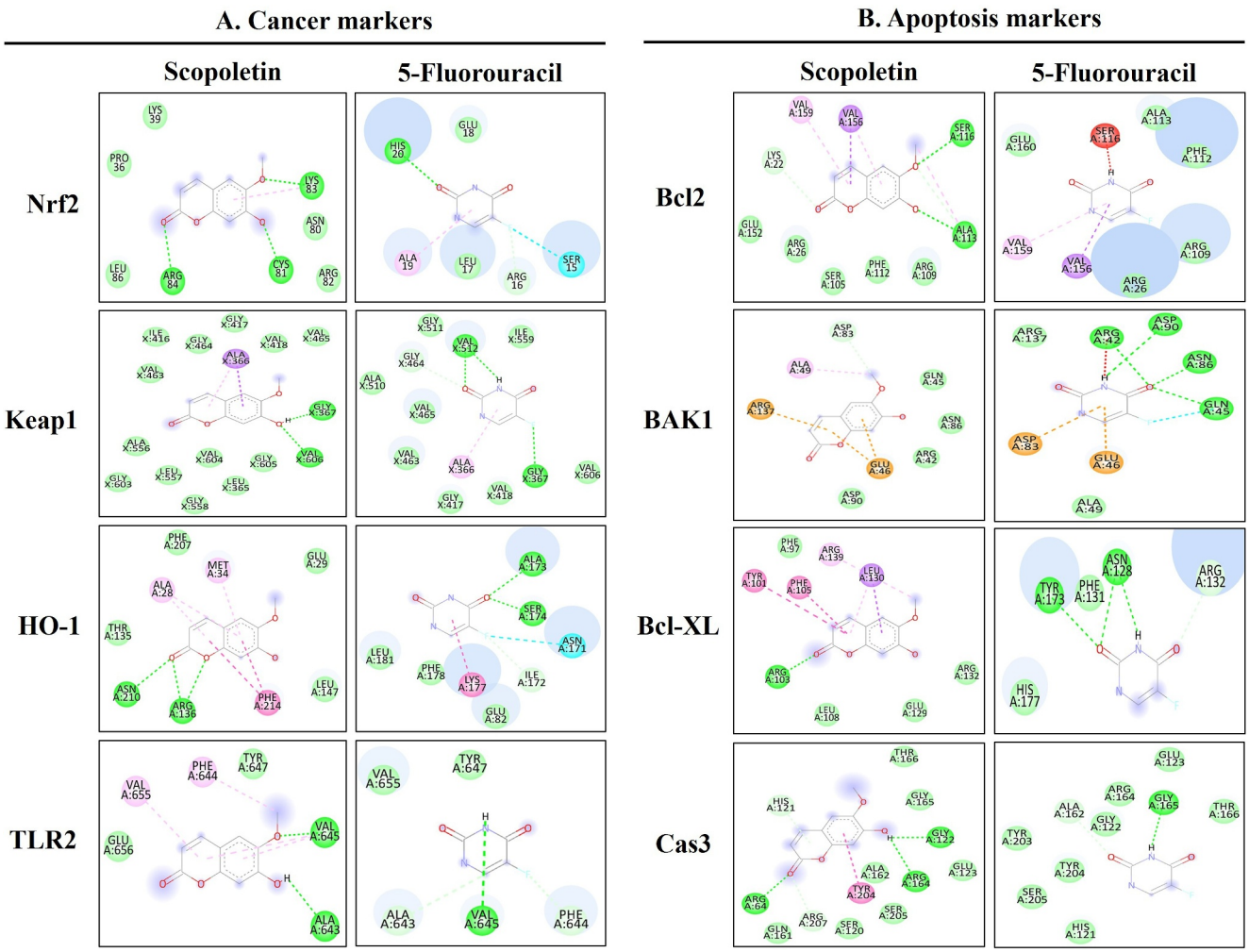

FIGURE 10 | 2D interaction complexes for cancer and apoptotic markers. 2D interaction complexes for (A) four cancer markers (Nrf-2, Keap-1, HO-1 and TLR-2) and (B) four apoptotic markers (Bcl-2, BAK1, Bcl-XL and Cas3). The image was obtained from Discovery Studio Visualizer of Scopoletin and 5-fluorouracil.

showing 71.8% cytotoxicity on HT-29 cells. Cell viability was also observed through trypan blue exclusion assay. Another study by Al-Abbas and Shaer (2021) displayed that HL60 cells exerts mortality with increase in concentration of the coumarin. Our study also observed a decrease in cell viability with the increase in concentration of the NEP-Sc.

In-silico molecular docking analysis was performed for Sc against some tumor-related proteins to find the interaction and binding affinity between Sc and the protein molecules. There are 15 protein targets (Nrf2, Keap1, HO1, TLR2, COX2, iNOS, TNF-α, STAT1, Caspase3, Bcl2, Bcl-XL, BAK1, LAMP3, LC3 and SIRT1) taken in this study. Sc shows good binding affinity against all these protein targets. Literature study showed that the interaction of Sc with the targets exerts positive feedback and relative gene expression.

Nuclear erythroid factor −2 (NEF2) related factor-2 (Nrf2) signaling pathway is an essential defence mechanism for oxidative injury and inflammation (Ahmed et al. 2017). Nrf2 is linked with reduced inflammation by inhibiting inflammatory mediators signal transducer and activator of transcription 1 (STAT1), inducible nitric oxide synthase (iNOS), interleukin-6 (IL-6) and regulatory mediators such as cyclooxygenase 2 (COX-2), tumor necrosis factor- α (TNF-α) by activating heme oxygenase 1 (HO-1), NADPH dehydrogenase [quinone] 1 (NQO1) (Dharshini et al. 2020). Nrf2 signaling pathway is an important defensive process against inflammation and oxidative stress. Sc activates Nrf2 exerting cytoprotective effects by the induction of various other related genes (Hassanein et al. 2020). Keap1, a negative regulator of Nrf2, inactivates the positive effect rendered by Nrf2. Simultaneous inhibition of Keap1 by Sc enhanced the translocation of Nrf2 into nucleus (Satoh et al. 2006). Nrf2 binds with musculoaponeurotic fibrosarcoma (Maf) and antioxidant response element (ARE) simulating the transcription of antioxidant genes leading to cell survival (Niture et al. 2010). This also activates defense genes namely HO-1 and NAD(P)H dehydrogenase [quinone] 1 (NQO1). Increasing the activity of defense genes decreases the production of iNOS and NO inhibiting ROS and oxidative stress

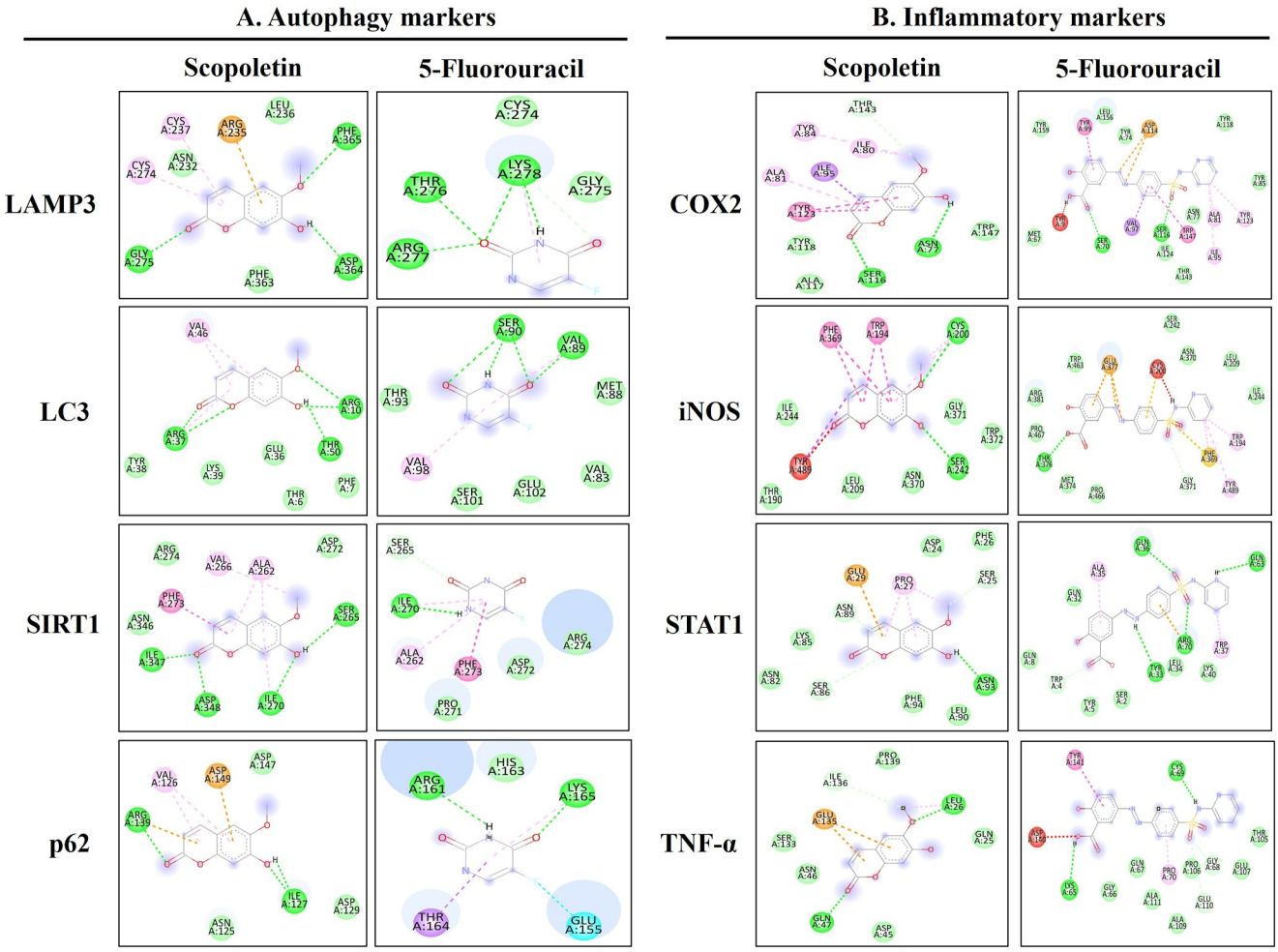

FIGURE 11 | 2D interaction complexes for autophagy and inflammatory markers. 2D interaction complexes for (A) four autophagy markers (LAMP3, LC3, SIRT1 and p62) and (B) four inflammatory markers (COX-2, iNOS, STAT-1 and TNF-Alpha). The image was obtained from Discovery Studio Visualizer of Scopoletin and 5-fluorouracil.

TABLE 2 | Binding affinity, binding mode, RMSD lower and upper bond calculation of standard drug (5-fluorouracil and sulfasalazine) and scopoletin.

Markers	Macromolecule	Ligand	Binding affinity (kcal/mol)	Binding mode	RMSD Lower bond	RMSD Upper bond
Cancer markers	Nrf2	Sc	−4.7	0	0	0
		5-Fluorouracil	−3.9	3	12.09	11.109
	Keap-1	Sc	−7.0	0	0	0
		5-Fluorouracil	−4.9	3	3.378	3.313
	HO-1	Sc	−5.8	1	4.926	1.272
		5-Fluorouracil	−4.4	3	3.046	1.654
	TLR2	Sc	−4.4	0	0	0
		5-Fluorouracil	−2.9	2	14.235	13.458
Apoptotic markers	Caspase 3	Sc	−6.3	0	0	0
		5-Fluorouracil	−4.2	4	30.139	29.847
	Caspase 7	Sc	−5.2	0	0	0
		5-Fluorouracil	−3.5	6	14.461	13.863
	Bcl2	Sc	−5.4	2	4.747	1.291

(Continues)

TABLE 2 | (Continued)

Markers	Macromolecule	Ligand	Binding affinity (kcal/mol)	Binding mode	RMSD Lower bond	RMSD Upper bond
		5-Fluorouracil	−4.3	4	16.537	15.717
	BAK1	Sc	−5.4	0	0	0
		5-Fluorouracil	−4.6	1	11.294	11.988
Autophagy markers	LAMP3	Sc	−4.7	2	29.07	26.288
		5-Fluorouracil	−4.2	1	2.472	2.122
	LC-3	Sc	−6.1	0	0	0
		5-Fluorouracil	−4.8	1	22.696	22.273
	SIRT1	Sc	−5.4	3	18.002	16.632
		5-Fluorouracil	−4.0	5	10.658	10.022
	p62	Sc	−4.2	5	17.98	17.513
		5-Fluorouracil	−3.7	2	16.817	16.55
Inflammatory markers	COX2	Sc	−6.9	0	0	0
		Sulfasalazine	−8.7	3	10.554	3.811
	iNOS	Sc	−6.6	2	26.099	23.589
		Sulfasalazine	−8.0	4	10.965	4.796
	STAT1	Sc	−5.0	4	19.615	18.425
		Sulfasalazine	−7.0	5	14.783	12.962
	TNF-α	Sc	−4.8	3	15.382	13.41
		Sulfasalazine	−6.5	1	5.334	3.752

TABLE 3 | Interaction of amino acids with of standard drug (5-fluorouracil and sulfasalazine) and scopoletin.

Markers	Macromolecule	Ligand	Interacting amino acids with the drug (5-fluorouracil and sulfasalazine) and scopoletin
Cancer markers	Nrf2	Sc	ASP83, ALA49, ARG137, GLU46
		5-Fluorouracil	ARG42, ASP90, ASN86, GLN45, ASP83, GLU46
	Keap-1	Sc	LYS22, VAL159, VAL156, SER116, ALA113
		5-Fluorouracil	SER116, VAL159, VAL156
	HO-1	Sc	TYR101, PHE105, LEU130, ARG139
		5-Fluorouracil	TYR173, ASN128, ARG132
	TLR2	Sc	ARG64, TYR204, ARG164, GLY122
		5-Fluorouracil	GLY165
Apoptotic markers	Caspase 3	Sc	TYR60, ASN61, LYS177
		5-Fluorouracil	ARG167
	Bcl-XL	Sc	ALA366, GLY367, VAL606
		5-Fluorouracil	ALA366, GLY367, GLY464, VAL512
	Bcl2	Sc	ARG235, ASN232, CYS237, CYS274, PHE365, GLY275, ASP364
		5-Fluorouracil	ARG277, LYS278, THR276
	BAK1	Sc	VAL46, ARG37, THR50, ARG10
		5-Fluorouracil	SER90, VAL89, VAL98
Autophagy markers	LAMP3	Sc	LYS83, CYS81, ARG84
		5-Fluorouracil	HIS20, ALA19, ARG16, SER15

(Continues)

TABLE 3 | (Continued)

Markers	Macromolecule	Ligand	Interacting amino acids with the drug (5-fluorouracil and sulfasalazine) and scopoletin
	LC-3	Sc	PHE273, ILE347, ASP348, ILE270, SER265, ALA262, VAL266
		5-Fluorouracil	ILE270, SER265, ALA262, PHE273
	SIRT1	Sc	VAL655, PHE644, VAL645, ALA643
		5-Fluorouracil	ALA643, VAL645, PHE644
	p62	Sc	ARG139, VAL126, ASP149, ASP147, ILE127
		5-Fluorouracil	ARG161, LYS165, THR164, GLU155
Inflammatory markers	COX2	Sc	THR143, TYR84, ILE80, ILE95, ALA81, TYR123, SER116, ASN77
		Sulfasalazine	TYR99, ASP114, TYR9, SER70, VAL97, SER116, TRP147, ALA81, ILE95, TYR123
	iNOS	Sc	PHE369, TRP194, CYS200, SER242, TYR489
		Sulfasalazine	THR376, GLU377, CYS200, PHE369, TRP194, TYR489
	STAT1	Sc	GLU29, PRO27, SER25, ASN93
		Sulfasalazine	ALA35, GLN36, GLN63, TYR33, ARG70, TRP37, TRP4
	TNF-α	Sc	GLU135, ILE136, LEU26, GLN47
		Sulfasalazine	ASP140, LYS65, TYR141, CYS69, PRO70, GLU110, GLY68

TABLE 4 | Binding energy calculation and percentage of resemblance of all genes of standard drug (5-fluorouracil and sulfasalazine) and scopoletin.

Markers	Macromolecule	Ligand	Binding affinity (kcal/mol)	BEDSA	Percentage of resemblance
Cancer markers	Nrf2	Sc	−4.7	0.8	33.33%
		5-Fluorouracil	−3.9		
	Keap-1	Sc	−7.0	1.1	100%
		5-Fluorouracil	−4.9		
	HO-1	Sc	−5.8	1.6	—
		5-Fluorouracil	−4.4		
	TLR2	Sc	−4.4	2.1	—
		5-Fluorouracil	−2.9		
Apoptotic markers	Caspase 3	Sc	−6.3	1.7	—
		5-Fluorouracil	−4.2		
	Bcl-XL	Sc	−5.4	3.9	50%
		5-Fluorouracil	−3.8		
	Bcl2	Sc	−5.4	0.5	—
		5-Fluorouracil	−4.3		
	BAK1	Sc	−5.4	1.3	—
		5-Fluorouracil	−4.6		
Autophagy markers	LAMP3	Sc	−4.7	0.8	—
		5-Fluorouracil	−4.2		
	LC-3	Sc	−6.1	1.4	100%
		5-Fluorouracil	−4.8		
	SIRT1	Sc	−5.4	1.5	100%

(Continues)

TABLE 4 | (Continued)

Markers	Macromolecule	Ligand	Binding affinity (kcal/mol)	BEDSA	Percentage of resemblance
		5-Fluorouracil	−4.0		
	p62	Sc	−4.2	0.5	—
		5-Fluorouracil	−3.7		
Inflammatory markers	COX2	Sc	−6.9	−2.2	40%
		Sulfasalazine	−8.7		
	iNOS	Sc	−6.6	−2.6	66.67%
		Sulfasalazine	−8.0		
	STAT1	Sc	−5.0	−3.0	—
		Sulfasalazine	−7.0		
	TNF-α	Sc	−4.8	−1.7	—
		Sulfasalazine	−6.5		

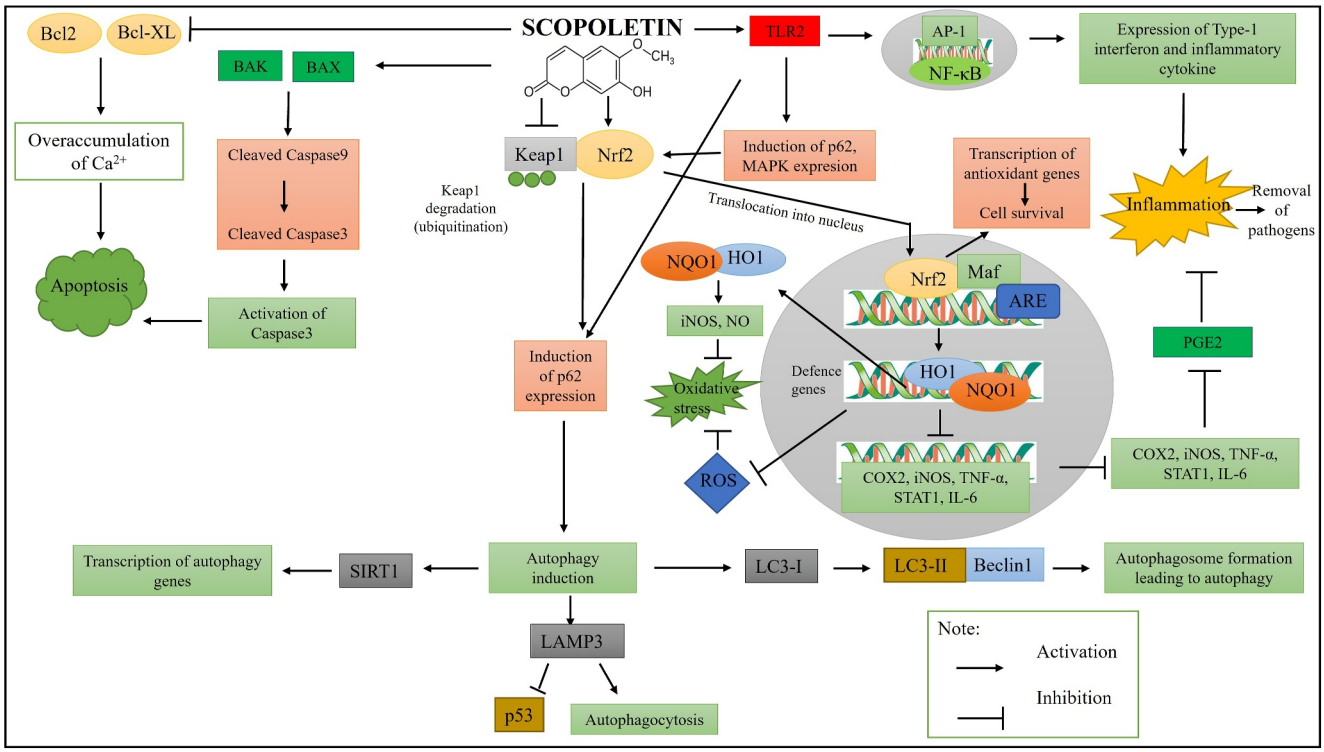

FIGURE 12 | NEP-Sc and its targeting genes. NEP-Sc might activate Nrf2 antioxidant pathway through the process of ubiquitination and inhibition of Keap1, thereby, Nrf2 translocation into nucleus takes place. Nrf2 interacts with Maf and ARE to transcribe antioxidant genes and enhance cell survival. Also, it simulates HO1 and NQO1, which exerts dual role including inhibition of inflammation through reduced generation of COX2, iNOS, STAT1, TNF-α and IL-6 and inhibition of oxidative stress by inhibiting iNOS, NO and ROS. TLR2 signaling enhance the immune response by initiating inflammation and clears the pathogens through AP1 and NF-κB activation. Both Nrf2 and TLR2 induces p62 expression which is required for autophagy activation. LC3, LAMP3 and SIRT1 exerts their role in simulating the formation of autophagosome leading to cell death. NEP-Sc activates BAX and BAK which cleaves cas9 and cas3 inducing apoptosis. It also inhibits Bcl2 and Bcl-XL- anti-apoptotic proteins and thereby overload of calcium in the cells leads to programmed cell death.

(Srisook et al. 2006). These antioxidant defense genes could block inflammatory mediators (PGE_2, TNF-α, STAT1 and IL-6) and regulatory enzymes (COX-2 and iNOS), thereby, inhibiting inflammation (Linton and Fazio 2003).

TLR2 signaling is important in the removal of pathogens by inducing inflammation. It also induces ubiquitin-binding protein (p62) and mitogen activated protein-kinase (MAPK) activating Nrf2. Nrf2 activates p62, which is an upstream gene of Nrf2 activating autophagy (Tao et al. 2015). Autophagy is an intracellular digestion process. Nrf2 induction of p62 activates LC3, LAMP3 and SIRT1. All these are related with the expression of autophagosome formation in digestion process (Vishnupriya et al. 2020). Apoptosis (programmed cell death) in

which Bcl-2 antagonist/killer 1 (BAK1), Bcl-2 associated X-Protein (BAX) and caspase 3 are involved in apoptosis process. B-cell lymphoma 2 (Bcl2) and B-cell lymphoma extra-large (Bcl-XL) are anti-apoptotic genes which is involved in apoptosis inhibition (Elmore 2007). To study about the pathways involved, Sc is docked with all these genes to evaluate for the binding affinity and its interaction. TLR2 induces the expression of p62, MAPK expression. p62 which is upstream of Nrf2 has the role in inhibiting Keap1 and activates Nrf2, a positive feedback loop (Komatsu et al. 2010). Induction of p62 activates autophagy. Autophagy related genes (LC3, LAMP3 and SIRT1) are activated and induces the formation of autophagosome leading to cell death. LC3 interacts with Beclin1 and induces autophagosome formation. LAMP3 induces autophagocytosis and also inhibits the expression of p53 tumor suppressor gene. SIRT1 after activation, transcribes all the autophagy related genes (Bednarczyk et al. 2017).

TLR2 signaling pathway is an innate immune response related pathway that protects host from external pathogens and internal compounds (Takeda and Akira 2005). Interaction of pathogen related antigen to TLR activates activator protein-1 (AP1) and nuclear factor κB (NF-κB). Sc also exerts similar function to TLR2 which expresses type-1 interferons and inflammatory cytokines like IL-6, interferon-γ, IL-12, TNF-α simulating inflammation and removes the pathogens (Tipping 2006).

Apoptosis is called as programmed cell death initiated by variety of death receptors that will enter into caspase cascade pathway leading to death of the cell (Lowe and Lin 2000). Sc activates the apoptotic genes namely BAK and BAX which simulates the caspase cascade pathway. In this pathway, caspase 9 is cleaved first which cleaves caspase 3 and initiates apoptosis. Sc inhibits Bcl2 and Bcl-XL-antiapoptotic proteins. The inhibition of Bcl2 over accumulates Ca2+, leading to apoptosis. The role of Bcl-XL is to inhibit apoptotic proteins, which were inhibited by scopoletin (Sakthivel et al. 2022). All these functions, roles, and interactions of Sc with protein targets are depicted in Figure 12.

5 | Conclusion

The present findings strongly suggest that the NEP-Sc has enhanced mechanical properties and surface-to-volume ratio in comparison with Sc. NEP-Sc was successfully prepared by nanoprecipitation technique. Future investigations will expand the study to include other well-characterized CRC cell lines, to validate the reproducibility of the observed effects, and assess inter-cell line variability.

Acknowledgments

The authors would like to thank the Department of Science and Technology—Anusandhan National Research Foundation (DST-ANRF), Government of India, for providing financial support to Dr. K.M. Sakthivel in the form of a Teachers Associateship for Research Excellence (TARE) (Ref. No: TAR/2023/000019).

Ethics Statement

The authors have nothing to report.

Consent

The authors have nothing to report.

Conflicts of Interest

The authors declare no conflicts of interest.

Data Availability Statement

All data generated during this study are included in this article.

References

Ahmed, S. M. U., L. Luo, A. Namani, X. J. Wang, and X. Tang. 2017. "Nrf2 Signaling Pathway: Pivotal Roles in Inflammation." *Biochimica et Biophysica Acta (BBA) - Molecular Basis of Disease* 1863, no. 2: 585–597. https://doi.org/10.1016/j.bbadis.2016.11.005.

Al-Abbas, N. S., and N. A. Shaer. 2021. "Combination of Coumarin and Doxorubicin Induces Drug-Resistant Acute Myeloid Leukemia Cell Death." *Heliyon* 7, no. 3: e06255. https://doi.org/10.1016/j.heliyon.2021.e06255.

Alam, F., N. U. Saqib, and Q. Waheed. 2017. "Cytotoxic Activity of Extracts and Crude Saponins From *Zanthoxylum armatum* DC. Against Human Breast (MCF-7, MDA-MB-468) and Colorectal (Caco-2) Cancer Cell Lines." *BMC Complementary and Alternative Medicine* 17: 1–9. https://doi.org/10.1186/s12906-017-1882-1.

Allémann, E., R. Gurny, and E. Doelker. 1993. "Drug-Loaded Nanoparticles: Preparation Methods and Drug Targeting Issues." *European Journal of Pharmaceutics and Biopharmaceutics* 39, no. 5: 173–191.

Asgar, M. A., G. Senawong, B. Sripa, and T. Senawong. 2015. "Scopoletin Potentiates the Anti-Cancer Effects of Cisplatin Against Cholangiocarcinoma Cell Lines." *Bangladesh Journal of Pharmacology* 10, no. 1: 69–77. https://doi.org/10.3329/bjp.v10i1.21202.

Bahuguna, A., I. Khan, V. K. Bajpai, and S. C. Kang. 2017. "MTT Assay to Evaluate the Cytotoxic Potential of a Drug." *Bangladesh Journal of Pharmacology* 12, no. 2: 115–118. https://doi.org/10.3329/bjp.v12i2.30892.

Bednarczyk, M., M. Muc-Wierzgon, N. Zmarzly, et al. 2017. "The Transcriptional Activity of LAMP3 Gene Involved in Autophagocytosis in Colorectal Cancer." *Journal of Biosciences and Medicines* 5, no. 12: 24. https://doi.org/10.4236/jbm.2017.512004.

Brar, B., K. Ranjan, A. Palria, et al. 2021. "Nanotechnology in Colorectal Cancer for Precision Diagnosis and Therapy." *Frontiers in Nanotechnology* 3: 699266. https://doi.org/10.3389/fnano.2021.699266.

Chan, F. K. M., K. Moriwaki, and M. J. De Rosa. 2013. "Detection of Necrosis by Release of Lactate Dehydrogenase Activity." *Immune Homeostasis: Methods and Protocols* 979: 65–70. https://doi.org/10.1007/978-1-62703-290-2_7.

Chen, X. T., and T. Wang. 2019. "Preparation and Characterization of Atrazine-Loaded Biodegradable PLGA Nanospheres." *Journal of Integrative Agriculture* 18, no. 5: 1035–1041. https://doi.org/10.1016/S2095-3119(19)62613-4.

da Paz, M. C., M. F. M. Almeida Santos, C. M. Santos, et al. 2012. "Anti-CEA Loaded Maghemite Nanoparticles as a Theragnostic Device for Colorectal Cancer." *International Journal of Nanomedicine* 7: 5271–5282. https://doi.org/10.2147/IJN.S32139.

Datta, K., S. Suman, S. Kumar, and A. J. Fornace Jr. 2016. "Colorectal Carcinogenesis, Radiation Quality, and the Ubiquitin-Proteasome Pathway." *Journal of Cancer* 7, no. 2: 174–183. https://doi.org/10.7150/jca.13387.

de Araujo Lopes, S. C., M. V. M. Novais, C. S. Teixeira, et al. 2013. "Preparation, Physicochemical Characterization, and Cell Viability Evaluation of Long-Circulating and pH-Sensitive Liposomes Containing Ursolic Acid." *BioMed Research International* 1: 467147. https://doi.org/10.1155/2013/467147.

Dharshini, L. C. P., S. Vishnupriya, K. M. Sakthivel, and R. R. Rasmi. 2020. "Oxidative Stress Responsive Transcription Factors in Cellular Signalling Transduction Mechanisms." *Cellular Signalling* 72: 109670. https://doi.org/10.1016/j.cellsig.2020.109670.

Elmore, S. 2007. "Apoptosis: A Review of Programmed Cell Death." *Toxicologic Pathology* 35, no. 4: 495–516. https://doi.org/10.1080/01926230701320337.

Gelperina, S., K. Kisich, M. D. Iseman, and L. Heifets. 2005. "The Potential Advantages of Nanoparticle Drug Delivery Systems in Chemotherapy of Tuberculosis." *American Journal of Respiratory and Critical Care Medicine* 172, no. 12: 1487–1490. https://doi.org/10.1164/rccm.200504-613PP.

Gul, A., Z. Akhter, F. Perveen, S. Kalsoom, F. L. Ansari, and M. Siddiq. 2019. "Molecular Docking and Quantitative Structure Activity Relationship (QSAR) Studies of Some Newly Synthesized Poly(Azomethine) Esters." *International Journal of Polymer Science* 1: 2103891. https://doi.org/10.1155/2019/2103891.

Gulbake, A., A. Jain, A. Jain, and S. K. Jain. 2016. "Insight to Drug Delivery Aspects for Colorectal Cancer." *World Journal of Gastroenterology* 22, no. 2: 582–599. https://doi.org/10.3748/wjg.v22.i2.582.

Hassanein, E. H., A. M. Sayed, O. E. Hussein, and A. M. Mahmoud. 2020. "Coumarins as Modulators of the Keap1/Nrf2/ARE Signaling Pathway." *Oxidative Medicine and Cellular Longevity* 1: 1675957. https://doi.org/10.1155/2020/1675957.

Hutchinson, R. A., R. A. Adams, D. G. McArt, M. Salto-Tellez, B. Jasani, and P. W. Hamilton. 2015. "Epidermal Growth Factor Receptor Immunohistochemistry: New Opportunities in Metastatic Colorectal Cancer." *Journal of Translational Medicine* 13: 1–11. https://doi.org/10.1186/s12967-015-0531-z.

Joshi, H., V. Gajera, and A. Katariya. 2021. "Review on Scopoletin: A Phenolic Coumarin With Its Medicinal Properties." *International Journal of Pharmaceutical Sciences and Research* 12, no. 7: 3567–3580. https://doi.org/10.13040/IJPSR.0975-8232.12(7).3567-80.

Kang, S. Y., S. H. Sung, J. H. Park, and Y. C. Kim. 1998. "Hepatoprotective Activity of Scopoletin, a Constituent of *Solanum lyratum*." *Archives of Pharmacal Research* 21, no. 6: 718–722. https://doi.org/10.1007/BF02976764.

Kheirelseid, E. A., N. Miller, and M. J. Kerin. 2013. "Molecular Biology of Colorectal Cancer: Review of the Literature." *American Journal of Molecular Biology* 3, no. 2: 1–9. https://doi.org/10.4236/ajmb.2013.32010.

Khuda-Bukhsh, A. R., S. S. Bhattacharyya, S. Paul, and N. Boujedaini. 2010. "Polymeric Nanoparticle Encapsulation of a Naturally Occurring Plant Scopoletin and Its Effects on Human Melanoma Cell A375." *Journal of Chinese Integrative Medicine* 8, no. 9: 853–862. https://doi.org/10.3736/jcim20100909.

Komatsu, M., H. Kurokawa, S. Waguri, et al. 2010. "The Selective Autophagy Substrate p62 Activates the Stress Responsive Transcription Factor Nrf2 Through Inactivation of Keap1." *Nature Cell Biology* 12, no. 3: 213–223. https://doi.org/10.1038/ncb2021.

Linton, M. F., and S. Fazio. 2003. "Macrophages, Inflammation, and Atherosclerosis." *International Journal of Obesity* 27, no. 3: S35–S40. https://doi.org/10.1038/sj.ijo.0802498.

Lowe, S. W., and A. W. Lin. 2000. "Apoptosis in Cancer." *Carcinogenesis* 21, no. 3: 485–495. https://doi.org/10.1093/carcin/21.3.485.

Manhattanadul, S., W. Ridtitid, S. Nima, N. Phdoongsombut, P. Ratanasuwon, and S. Kasiwong. 2011. "Effects of *Morinda citrifolia* Aqueous Fruit Extract and Its Biomarker Scopoletin on Reflux Esophagitis and Gastric Ulcer in Rats." *Journal of Ethnopharmacology* 134, no. 2: 243–250. https://doi.org/10.1016/j.jep.2010.12.004.

Mogana, R., T.-J. Kang, and C. Wiart. 2013. "Anti-Inflammatory, Anticholinesterase, and Antioxidant Potential of Scopoletin Isolated From *Canarium patentinervium* Miq. (Burseraceae Kunth)." *Evidence-Based Complementary and Alternative Medicine* 1: 734824. https://doi.org/10.1155/2013/734824.

Mohammadinejad, S., A. Akbarzadeh, M. Rahmati-Yamchi, et al. 2015. "Preparation and Evaluation of Chrysin Encapsulated in PLGA-PEG Nanoparticles in the T47-D Breast Cancer Cell Line." *Asian Pacific Journal of Cancer Prevention* 16, no. 9: 3753–3758. https://doi.org/10.7314/apjcp.2015.16.9.3753.

Niture, S. K., J. W. Kaspar, J. Shen, and A. K. Jaiswal. 2010. "Nrf2 Signaling and Cell Survival." *Toxicology and Applied Pharmacology* 244, no. 1: 37–42. https://doi.org/10.1016/j.taap.2009.06.009.

Oršolić, N., I. Kosalec, and I. Bašić. 2005. "Synergistic Antitumor Effect of Polyphenolic Components of Water-Soluble Derivative of Propolis Against Ehrlich Ascites Tumour." *Biological and Pharmaceutical Bulletin* 28, no. 4: 694–700. https://doi.org/10.1248/bpb.28.694.

Prisciandaro, E., G. Sedda, A. Cara, C. Diotti, L. Spaggiari, and L. Bertolaccini. 2023. "Artificial Neural Networks in Lung Cancer Research: A Narrative Review." *Journal of Clinical Medicine* 12, no. 3: 880. https://doi.org/10.3390/jcm12030880.

Reheman, D., J. Zhao, S. Guan, G. C. Xu, Y. J. Li, and S. R. Sun. 2020. "Apoptotic Effect of Novel Pyrazolone-Based Derivative [Cu (PMPP-SAL)(EtOH)] on HeLa Cells and Its Mechanism." *Scientific Reports* 10, no. 1: 18235. https://doi.org/10.1038/s41598-020-75173-8.

Repetto, G., A. Del Peso, and J. L. Zurita. 2008. "Neutral Red Uptake Assay for the Estimation of Cell Viability/Cytotoxicity." *Nature Protocols* 3, no. 7: 1125–1131. https://doi.org/10.1038/nprot.2008.75.

Sakthivel, K. M., S. Vishnupriya, L. C. Priya Dharshini, R. R. Rasmi, and B. Ramesh. 2022. "Modulation of Multiple Cellular Signaling Pathways as Targets for Anti-Inflammatory and Anti-Tumorigenesis Action of Scopoletin." *Journal of Pharmacy and Pharmacology* 74, no. 2: 147–161. https://doi.org/10.1093/jpp/rgab047.

Sallal, H. A., A. A. Abdul-Hamead, and F. M. Othman. 2020. "Effect of Nano Powder (Al_2O_3-CaO) Addition on the Mechanical Properties of the Polymer Blend Matrix Composite." *Defence Technology* 16, no. 2: 425–431. https://doi.org/10.1016/j.dt.2019.07.013.

Satoh, T., S. I. Okamoto, J. Cui, et al. 2006. "Activation of the Keap1/Nrf2 Pathway for Neuroprotection by Electrophilic Phase II Inducers." *Proceedings of the National Academy of Sciences* 103, no. 3: 768–773. https://doi.org/10.1073/pnas.0505723102.

Srisook, K., S. S. Han, H. S. Choi, et al. 2006. "CO From Enhanced HO Activity or From CORM-2 Inhibits Both O_2− and NO Production and Downregulates HO-1 Expression in LPS-Stimulated Macrophages." *Biochemical Pharmacology* 71, no. 3: 307–318. https://doi.org/10.1016/j.bcp.2005.10.042.

Strober, W. 1997. "Trypan Blue Exclusion Test of Cell Viability." *Current Protocols in Immunology* 21, no. 1: A–3B. https://doi.org/10.1002/0471142735.ima03bs21.

Sulaiman, G. M., M. S. Jabir, and A. H. Hameed. 2018. "Nanoscale Modification of Chrysin for Improved Therapeutic Efficiency and Cytotoxicity." Supplement, *Artificial Cells, Nanomedicine and Biotechnology* 46, no. sup1: 708–720. https://doi.org/10.1080/21691401.2018.1434661.

Tabana, Y. M., L. E. A. Hassan, M. B. K. Ahamed, et al. 2016. "Scopoletin, an Active Principle of Tree Tobacco (*Nicotiana glauca*) Inhibits Human Tumor Vascularization in Xenograft Models and Modulates ERK1, VEGF-A, and FGF-2 in Computer Model." *Microvascular Research* 107: 17–33. https://doi.org/10.1016/j.mvr.2016.04.009.

Takeda, S., and A. Akira. 2005. "Toll-Like Receptors in Innate Immunity." *International Immunology* 17, no. 1: 1–14. https://doi.org/10.1093/intimm/dxh186.

Tao, S., S. L. Park, M. R. de la Vega, D. D. Zhang, and G. T. Wondrak. 2015. "Systemic Administration of the Apocarotenoid Bixin Protects Skin Against Solar UV-Induced Damage Through Activation of NRF2." *Free Radical Biology and Medicine* 89: 690–700. https://doi.org/10.1016/j.freeradbiomed.2015.08.028.

Thangavelu, K., F. Ravaux, and L. Zou. 2021. "Cellulose Acetate-MoS_2 Amphiphilic Janus-Like Fibrous Sponge for Removing Oil From Wastewater." *Environmental Technology & Innovation* 24: 101870. https://doi.org/10.1016/j.eti.2021.101870.

Thangavelu, K., and L. Zou. 2022. "Evaluating Oil Removal by Amphiphilic MoS_2/Cellulose Acetate Fibrous Sponge in a Flow-Through Reactor and by Artificial Neural Network." *Environmental Nanotechnology, Monitoring & Management* 18: 100684. https://doi.org/10.1016/j.enmm.2022.100684.

Tipping, P. G. 2006. "Toll-Like Receptors: The Interface Between Innate and Adaptive Immunity." *Journal of the American Society of Nephrology* 17, no. 7: 1769–1771. https://doi.org/10.1681/ASN.2006050489.

Vishnupriya, S., L. C. P. Dharshini, K. M. Sakthivel, and R. R. Rasmi. 2020. "Autophagy Markers as Mediators of Lung Injury-Implication for Therapeutic Intervention." *Life Sciences* 260: 118308. https://doi.org/10.1016/j.lfs.2020.118308.

Wei, Y., J. Liang, X. Zheng, et al. 2017. "Lung-Targeting Drug Delivery System of Baicalin-Loaded Nanoliposomes: Development, Biodistribution in Rabbits, and Pharmacodynamics in Nude Mice Bearing Orthotopic Human Lung Cancer." *International Journal of Nanomedicine* 12: 251–261. https://doi.org/10.2147/IJN.S119895.

Yashaswee, S., and S. K. Trigun. 2020. "Cytotoxicity and Induction of Apoptosis in Melanoma (MDA-MB-435S) Cells by Emodin." *Journal of Scientific Research* 64, no. 2: 158–166. https://doi.org/10.37398/JSR.2020.640223.

Yu, S. M., D. H. Hu, and J. J. Zhang. 2015. "Umbelliferone Exhibits Anticancer Activity Via the Induction of Apoptosis and Cell Cycle Arrest in HepG2 Hepatocellular Carcinoma Cells." *Molecular Medicine Reports* 12, no. 3: 3869–3873. https://doi.org/10.3892/mmr.2015.3797.